

RESEARCH ARTICLE

OPEN ACCESS






INVESTIGATIVE ANALYSIS OF SELECTED FSO MODELS WITH VARYING WAVELENGTHS FOR TROPICAL WEATHER

Ibukunoluwa A. Olajide*¹, Samson A. Oyetunji², Yekeen O. Olasoji³, Wasiu O. Popoola⁴ and Muhammad Ijaz⁵

^{1,2,3} Department of Electrical and Electronics Engineering, The Federal University of Technology, Akure, Nigeria.

⁴ Institute for Digital communication, University of Edinburgh, United Kingdom.

⁵ Department of Electrical and Electronics Engineering, Manchester Metropolitan University, United Kingdom.

¹ <http://orcid.org/0000-0001-9647-876X> , ² <http://orcid.org/0000-0001-8171-0327> , ³ <http://orcid.org/0000-0002-1978-1930> ,
⁴ <http://orcid.org/0000-0002-2954-7902> , ⁵ <http://orcid.org/0000-0002-0050-9435> 

Email: *iaadebanjo@futa.edu.ng, saoyetunji@futa.edu.ng, yoolasoji@futa.edu.ng, w.popoola@ed.ac.uk, m.ijaz@mmu.ac.uk

ARTICLE INFO

Article History

Received: March 14th, 2023

Accepted: April 26th, 2023

Published: April 29th, 2023

Keywords:

Scattering,
Visibility,
Attenuation,
Rain Intensity.

ABSTRACT

In this paper, an investigation of some selected Mie and geometric Scattering models for free space optical (FSO) communication was done on available atmospheric data in Nigeria. The Kim and Kruse models have been established for the temperate region. In this work, the models were examined using the visibility data from the year 2008 to 2019. The models were examined under the 2% and 5% transmission threshold and under the wavelengths 780nm, 850nm, 1100nm, and 1550nm. The results indicates a higher attenuation at 780nm, supporting what is available in literature. The Suriza et al, ITU-R(Carbonneau) and Gailani et al models were investigated using the rain intensity data. The Suriza et al model indicates a reduced attenuation compared to the other two models.



Copyright ©2023 by authors and Galileo Institute of Technology and Education of the Amazon (ITEGAM). This work is licensed under the Creative Commons Attribution International License (CC BY 4.0).

I. INTRODUCTION

Free space optical (FSO) communication is a recent technology in wireless communication that is gradually becoming explorable and deplorable. Emergence of Internet of Things (IoT) and increased demand for internet penetration has resulted in unending congestion of the Radio Frequency (RF) spectrum. The effect on licensed band is high cost of data transfer. This is compounded by the cost of infrastructural deployment of optical fiber cables. In handling this bottleneck, an alternative technological approach is to be considered to ease off the strain on RF infrastructure. The need to develop a viable alternative becomes inevitable if the desire to increase penetration and teledensity which are the fulcrum of digital economy is to be realized even with population growth. Free space optical communication (FSO) was developed in response to the increase in demand for high speed and tap- proof communication system [1]. It is a promising communication technique that has great advantage in handling losses, security issues, central connectivity, spectrum, and bandwidth management. Radio frequency (RF) and Millimeter

wave technologies offer data rates from tens mbps to several Hundreds mbps, but spectrum congestion, license issues and unwanted interference from other bands are their known limitations, though emerging license-free bands of RF technology stand promising, yet bandwidth limitation places FSO ahead as a substitute to address the last and first mile problem in wireless communication [2]. Despite the huge advantages of FSO, it has its peculiar disadvantages. Due to the narrowness of its beams, stiff alignment and pointing is required to prevent beam dispersion [4][5]. Another principal factor of limitation is the effect of the propagating medium- the atmosphere. FSO suffers easily from absorption, rain, fog, and snow -general atmospheric condition and turbulence. Nigeria as a tropical country has its inherent climatic conditions that is needed to be studied in order to implement the free space optical communication technology. In this paper, a fundamental and investigative study of established Mie and Geometric scattering models in FSO were used on sets of atmospheric data obtained for Akure, Nigeria. Kim and Kruse models were examined under the 2% and 5% transmission

threshold for the wavelengths 780nm, 850nm, 1100nm, and 1550nm. The results indicates a higher attenuation at 780nm. The Suriza et al, ITU-R (Carbonneau) and Gailani et al models were investigated using the rain intensity data. The Suriza et al model gave a reduced attenuation compared to the other two models. It provides a preliminary analysis of simulated results of what to expect when a thorough experimental analysis is carried out within the southern region of Nigeria. The paper is organized as follows: literature review is presented in Section II, the methodological approach is provided in Section III, while the graphical analysis and discussion is given in Section IV. The conclusion is drawn in Section V.

II. THEORETICAL REFERENCE

II.1 FSO LOSSES

Propagated power from an FSO transmitter to the receiver is affected by various factors. They are system loss, Geometric and misalignment losses, atmospheric losses, atmosphere turbulence induced fading, and ambient noise [5]. All these losses do have relative to high effects on FSO propagation, but the scope of this study is atmospheric losses.

II.1.1 Atmospheric Losses

The Earth's surface layers are broadly classed into two spheres: Homosphere and the Heterosphere. The Homosphere ranges from 0-9 km while the Heterosphere is above 90 km [4]. The Homosphere is where free space optical communication takes place. Furthermore, the Homosphere can be classed / divided into (i) Troposphere (0-20 km), (ii) Stratosphere (20-50 km) and Mesosphere (50-90 km). The Homosphere is resident to many gases, water vapours, pollutants and chemicals. These tenants of the Homosphere induce atmosphere effects on the propagated signals, whether RF or IR signals. These interaction causes absorption and scattering of the signals leading to signal attenuation. Beers Law expresses the attenuation of travelling light through the atmosphere under the influence of absorption and scattering [6][3]. According to Beers Law, the transmission, τ of radiation in the atmosphere as a function of distance, d is given as [6],

$$\tau = \exp(-\gamma d) \tag{1}$$

where $\tau = \frac{I_R}{I_0}$, which could be called atmospheric attenuation, γ is the attenuation/extinction coefficient. γ is the sum of the absorption and the scattering coefficients from aerosols and molecular constituents, given as [2].

$$\gamma = \alpha_m + \alpha_a + \beta_m + \beta_a \tag{2}$$

The first two terms represents the molecular and aerosol absorption while the last two, the molecular and aerosol scattering.

II.1.2 Absorption

Absorption is caused by the collision of photons with various dispersed liquid and solid particles in the atmosphere [3]. Some of these photons are extinguished, and energy is absorbed [7]. Atmospheric absorption is a wavelength-dependent phenomenon, therefore, it is selective. These absorbing particles are divided into Molecule and Aerosol absorbers [4]. Molecule absorbers are Nitrogen, Hydrogen, Ozone, Oxygen, Carbon dioxide etc.; they are gases present in the atmosphere. Aerosols are suspended particles in the medium [7]. The suspended particles could be liquid or solid particles. Liquid particles are mist and water vapour, while solid particles are dust, smoke, volcanic particles, maritime droplets. These particles create reducing effects on optical link margin, and link availability.

Absorption causes the atmosphere to have transparent zones, called atmospheric transmission windows [2][3]. This transmission window allows specific frequencies of light to pass through it. However, the wavelength of transmission is usually chosen to match the atmospheric transmission window, thereby resulting in the attenuation / extinction coefficient being a scattering parameter alone. Therefore, Equation (2) becomes.

$$\gamma = \beta_a \tag{3}$$

II.1.3 Scattering

Scattering occurs when the optical beam collides with a scatterer. This leads to a redistribution of light or deflection in angle of beam arrival [7]. As light is redistributed, optical energy is redistributed with and without wavelength change [4]. The redistribution leads to reduction in the intensity of beam for longer distance [8]. The scattering effect depends on the radius, r of the particles (fog, aerosol) experienced during propagation [2]. There are three main types of scattering: Rayleigh, Mie, and Non-Selective scattering.

In Rayleigh scattering, the size of the colliding particle is less than the wavelength of the beam. For Rayleigh, $x_0 \ll 1$; therefore, it is known as Molecule scattering [8].

In Mie scattering, the size of the colliding particle is comparable to the wavelength of the beam, $x_0 \approx 1$. In the Non-selective scattering also known as geometric scattering, the colliding particles size is larger than the wavelength of the beam, $x_0 \gg 1$ [9]. A summary of typical atmospheric scattering particles is presented in Table 1.

Table 1: Atmospheric Scattering Particles.

Type	Radius(μ m)	Size Parameter, x_0	Scattering Process
Air Molecules	0.0001	0.00074	Rayleigh
Haze particle	0.01-1	0.074-7.4	Rayleigh – Mie
Fog droplets	1-20	7.40-147.8	Mie– Geometric
Rain	100-10000	740-74000	Geometric/ Non-Selective
Snow	1000-5000	7400-37000	Geometric/Non-Selective
Hail	5000-50000	37000-50000	Geometric/Non-Selective

Source: Ghassemlooy and Popoola, (2010), Kim et al (2001).

II.1.4 Atmosphere Turbulence

The variation in the temperature, wind, and pressure of air sets a random phenomenon, which is spatial and temporal fluctuations of refractive index [7]. This turbulence results in eddies, cells or air particles having varying sizes from 0.1 m to 10 m. These eddies deflect optical transmission path. Atmospheric turbulence depends on (i) atmospheric pressure/ altitude (ii) wind speed, and (iii) variation of index of refraction [2]. When a plane wave passes through these eddies, part of the wave are reflected causing a distorted wave with varied intensity, and a warping of the isophase surface [3]. This is shown from the relationship between temperature, pressure and refractive index:

$$n \approx 79 \times \frac{P}{T} \quad (4)$$

where P is the atmosphere pressure is [mbar], T is the temperature in kelvin [K].

Atmosphere turbulence is measured in terms of refractive index structure coefficient, C_n^2 [7]. It is the most important parameter for the checking turbulence strength. C_n^2 depends on geographical location, altitude and time of the day. The value of C_n^2 for weak turbulence at ground level could be little as $10^{-17} \text{m}^{-2/3}$, and for a strong turbulence, it can be up to $10^{-13} \text{m}^{-2/3}$ [7]. Some of the commonly used models are presented in [11].

III. MATERIALS AND METHODS

III.1 MIE SCATTERING

Characterisation of atmospheric Mie scattering was carried out using MATLAB. Two established models will be investigated to check the suitability to the atmospheric structure of the selected region

III.1.1 Kim and Kruse Model

The prediction of fog attenuation based on visibility was employed for this work. The Koschmieder law expresses the visibility by the extinction coefficient at 550 nm. At 550 nm, visibility is given as [12]:

$$V = \frac{\ln\left[\frac{1}{\tau_{th}}\right]}{\gamma(\lambda_0)} \quad (5)$$

where τ_{th} is transmission threshold over the atmospheric path, γ is the extinction coefficients (km^{-1}), and λ_0 equals 550 nm. The specific attenuation α can be expressed in terms of the visibility range, thereby as

$$\alpha = \frac{\log[1/\tau_{th}]}{V} \quad (6)$$

For the prediction of the fog attenuation, the following equation was considered:

$$\beta_a(\lambda) \approx \gamma(\lambda) = \frac{\ln\left[\frac{1}{\tau_{th}}\right]}{V} \left[\frac{\lambda}{\lambda_0}\right]^{-q} \quad (7)$$

where τ_{th} is the transmission threshold and it was taken as 2% and 5% of the transmitted power for this study, λ_0 is the maximum spectrum at 550 nm, V is the visibility, and q is the coefficient of particle size distribution. The values of q will be taken as noted by Kim and Kruse to be [13].

$$q = \begin{cases} 1.6 & \text{for } V > 50 \text{ km} \\ 1.3 & \text{for } 6 < V < 50 \text{ km} \\ 0.16V + 0.34 & \text{for } 1 < V < 6 \text{ km} \\ V - 0.5 & \text{for } 0.5 < V < 1 \text{ km} \\ 0 & \text{for } V < 0.5 \text{ km} \end{cases} \quad (8)$$

III.2 NON-SELECTIVE SCATTERING

Raindrops do have transient effects on optical signals. In the tropics, heavy rain is the major cause of attenuation of an FSO link [14]. Usually, the rain intensity data is often used to determine the specific rain attenuation in FSO. The international Telecommunication union sector (ITU-R- Carbonneau), Suriza et al, and Gailani et al model [14] was examined in this research. These models are based on rain rate distribution, but other prediction models exist which are based on rain-drop size distribution, which may not appropriately apply to the tropical region [13]. Rain specific attenuation is represented by the Power Law [16]:

$$A = kR^\alpha \quad (9)$$

where R is the rain rate in millimeter per hour, k and α are power law parameters.

Power law parameters are frequency, rain drop size and rain temperature dependent, therefore it will be assumed that rain drop size is oblong. Table II gives the parameters of the adopted models.

Table 2: Selected Rain Models.

Rain Model	k	α	Region
Carbonneau	1.076	0.67	Temperate
Gailini et al	2.03	0.70	Tropics
Suriza et al	0.3988	0.7601	Tropics

Source: Authors, (2023).

IV. RESULTS AND DISCUSSIONS

IV.1 MIE SCATTERING

Visibility data was obtained from The World Weather Online in Hong Kong for Akure, from July 2008 to October 2022. The historical data runs for 12 years. Definite analysis of the data was done using two known models in Mie scattering- KIM and Kruse models. Analytical examination of data sets was done on yearly basis under varying parameters.

Yearly Analysis with varying wavelengths was carried out and is observed in figure 1 to Figure 17.

The transmission threshold τ_{th} at 2 % is presented and a comparison is made with a transmission threshold at 5 % Four (4) operating transmission windows, namely 780nm, 850nm, 1100nm and 1550nm were used for comparison. Figure 1 gives the result for varying transmission window when τ_{th} at 2% for the year 2011. The result shows a general trend in the relationship between attenuation (dB/km) and visibility (km). Selected plots are presented in this paper. The transmission window of 1550nm performs best for both models giving a reduced equivalent attenuation. This result agrees with theoretical postulations.

The graph obtained for the year 2014 given in Figure 3, shows an even distribution with a similar resemblance to what was obtained in the year 2011. Figure 4 gives the graphical analysis of the years 2016. It is also observed that the curve appears closer in the year 2012 (Figure 2) and 2016 due to the closeness of the visibility data obtained for those years. At transmission window of 780 nm, the highest attenuation in dB/km is observed for all results

presented. A combined graph of τ_{th} at 2% and 5% is presented in Figure 5. The plots obtained for the years have a close segmentation observed. It is observed that the attenuation obtained at transmission window of 1550 nm when τ_{th} is at 5% lies closely in attenuation value obtained at transmission window of 1100 nm when τ_{th} is at 2%. Further observed, is the closeness in attenuation values of the models at varied value of τ_{th} . It is noted from the results obtained that from visibility of 6 km upwards, the attenuation in dB/km for both models at either 2% or 5% of τ_{th} are the same. This is in accordance with the rules guiding the usage of the models. At this level, the only point of argument for any reasonable deployment of FSO is the choice value of τ_{th} .

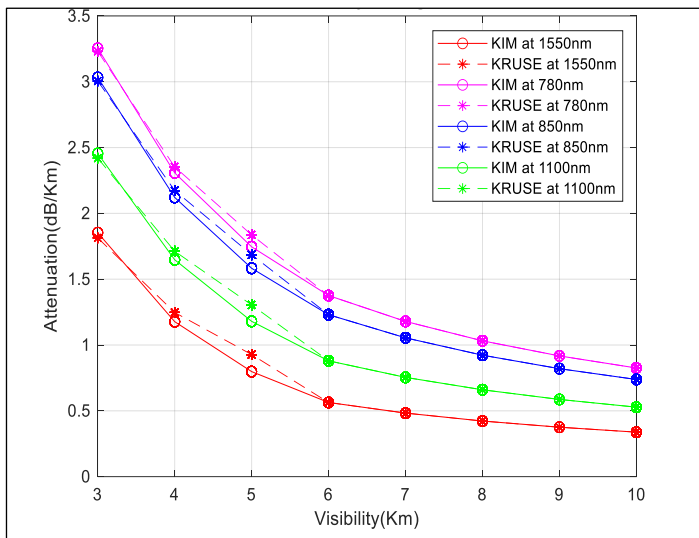


Figure 1: Varied transmission window for attenuation/visibility performance for the year 2011 @ $\tau_{th} = 2\%$. Source: Authors, (2023).

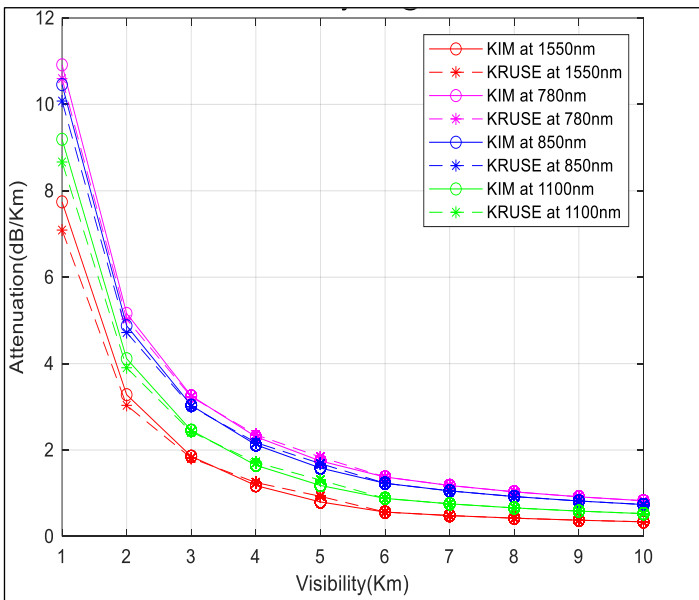


Figure 2: Varied transmission window for attenuation/visibility performance for the year 2012 @ $\tau_{th} = 2\%$. Source: Authors, (2023).

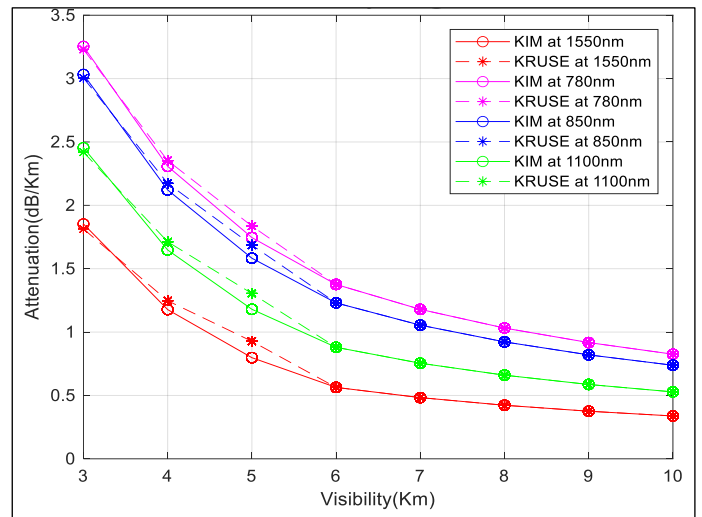


Figure 3: Varied transmission window for attenuation/visibility performance for the year 2014 @ $\tau_{th} = 2\%$. Source: Authors, (2023).

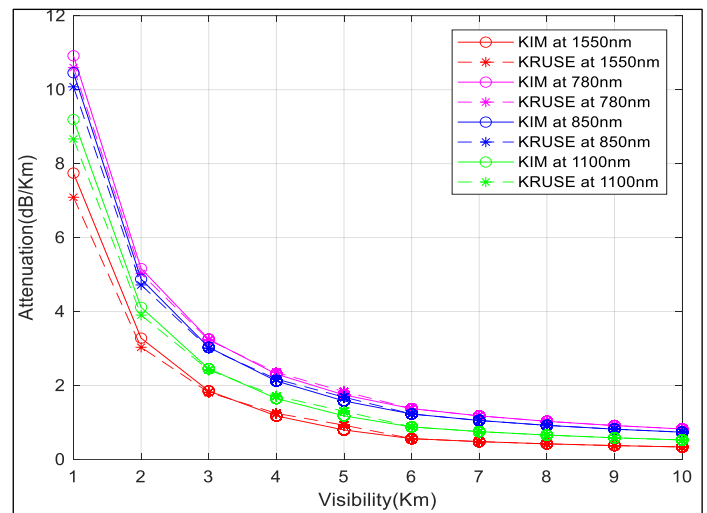


Figure 4: Varied transmission window for attenuation/visibility performance for the year 2016 @ $\tau_{th} = 2\%$. Source: Authors, (2023).

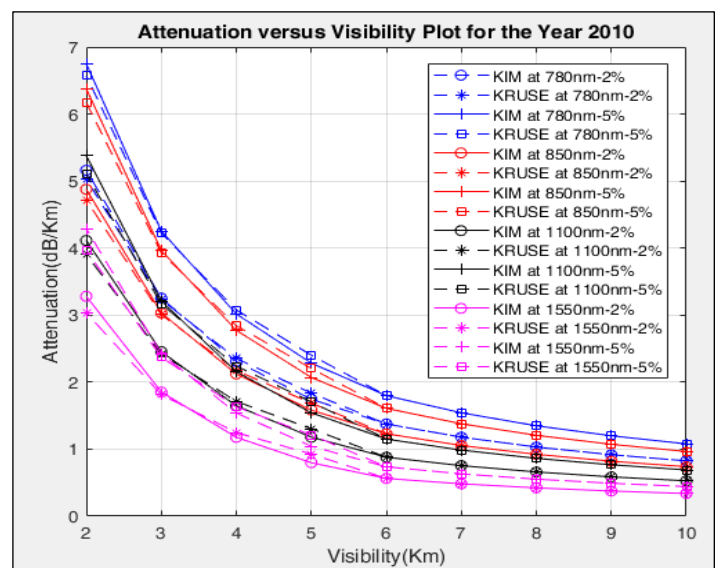


Figure 5: Combined attenuation plot when τ_{th} is at 2% and 5% for the year 2019. Source: Authors, (2023)

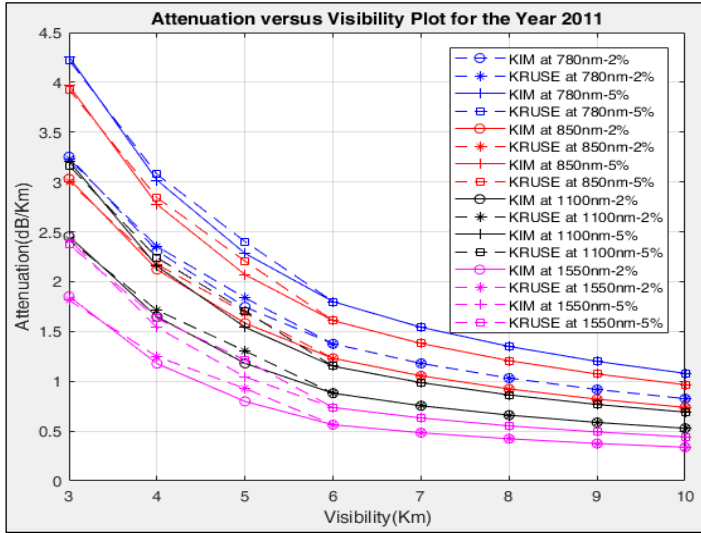


Figure 6: Combined attenuation plot when τ_{th} is at 2% and 5% for the year 2019. Source: Authors, (2023).

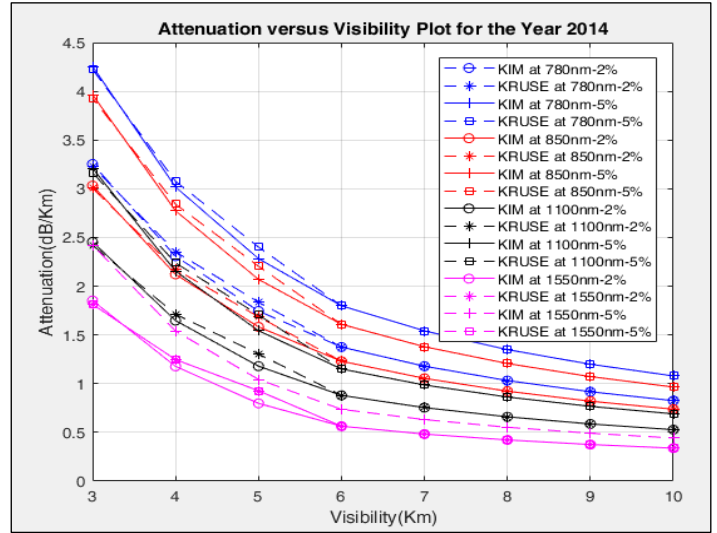


Figure 9: Combined attenuation plot when τ_{th} is at 2% and 5% for the year 2019. Source: Authors, (2023).

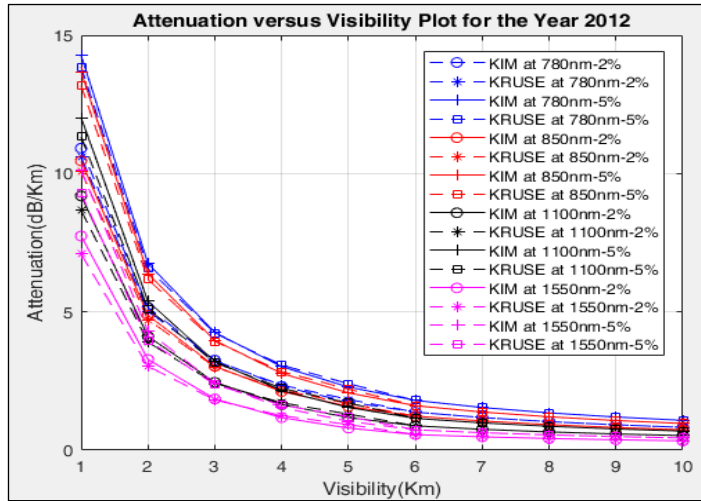


Figure 7: Combined attenuation plot when τ_{th} is at 2% and 5% for the year 2019. Source: Authors, (2023).

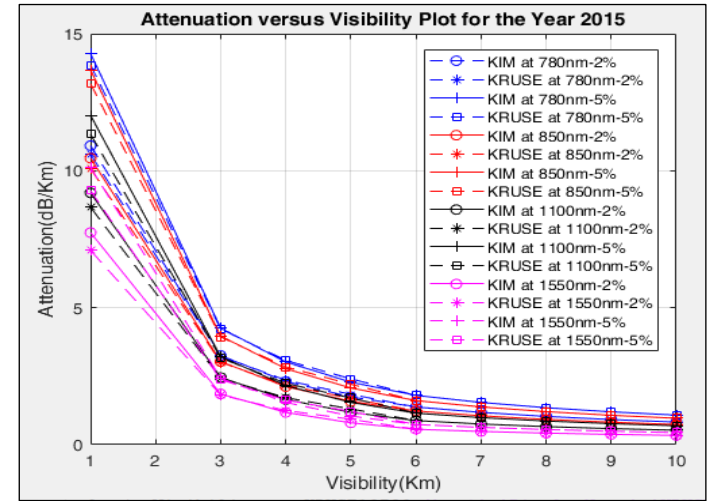


Figure 10: Combined attenuation plot when τ_{th} is at 2% and 5% for the year 2019. Source: Authors, (2023).

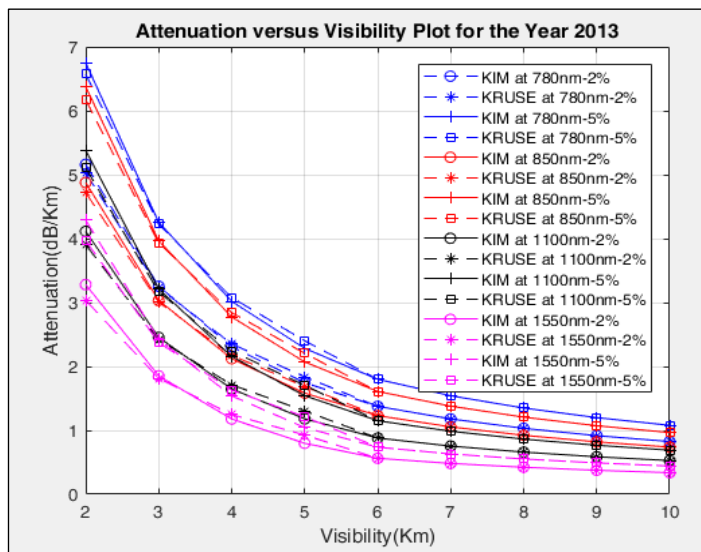


Figure 8: Combined attenuation plot when τ_{th} is at 2% and 5% for the year 2019. Source: Authors, (2023).

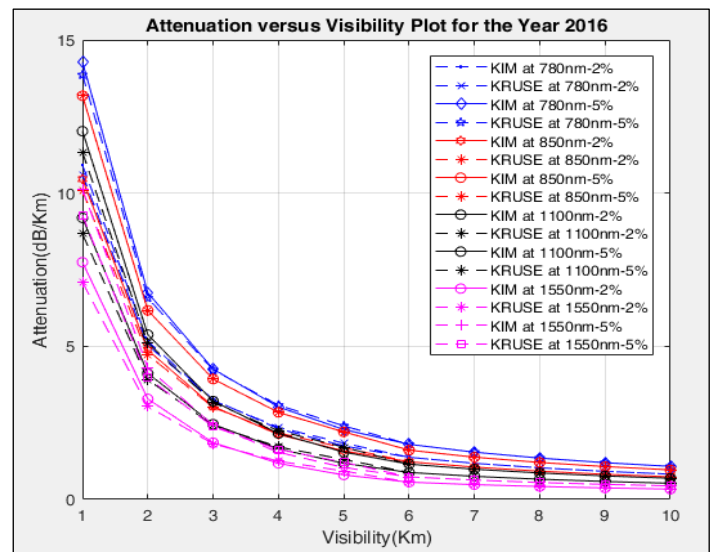


Figure 11: Combined attenuation plot when τ_{th} is at 2% and 5% for the year 2019. Source: Authors, (2023).

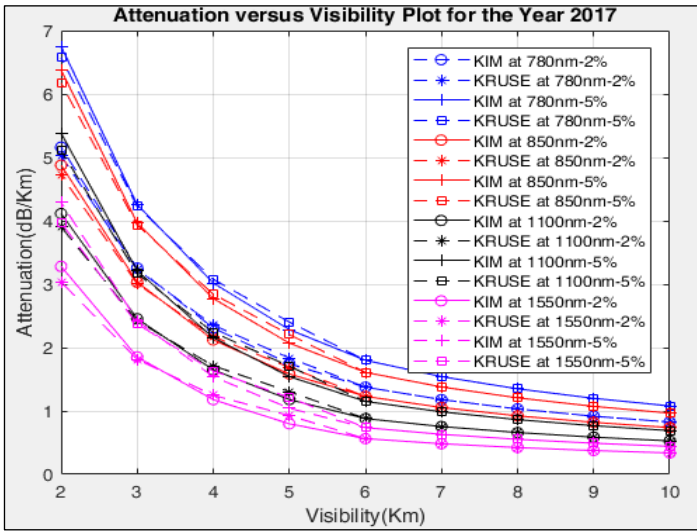


Figure 12: Combined attenuation plot when τ_{th} is at 2% and 5% for the year 2019. Source: Authors, (2023).

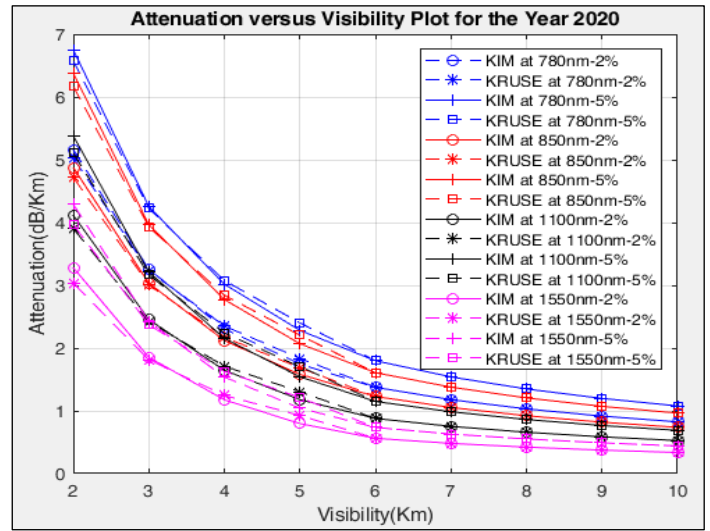


Figure 15: Combined attenuation plot when τ_{th} is at 2% and 5% for the year 2019. Source: Authors, (2023).

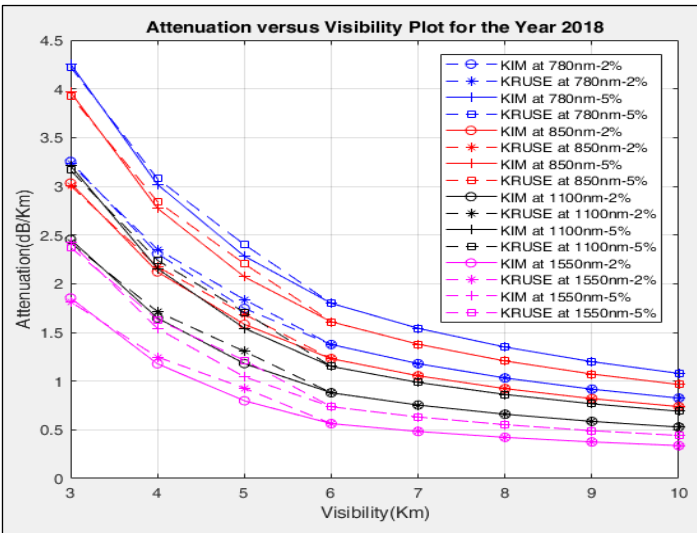


Figure 13: Combined attenuation plot when τ_{th} is at 2% and 5% for the year 2019. Source: Authors, (2023).

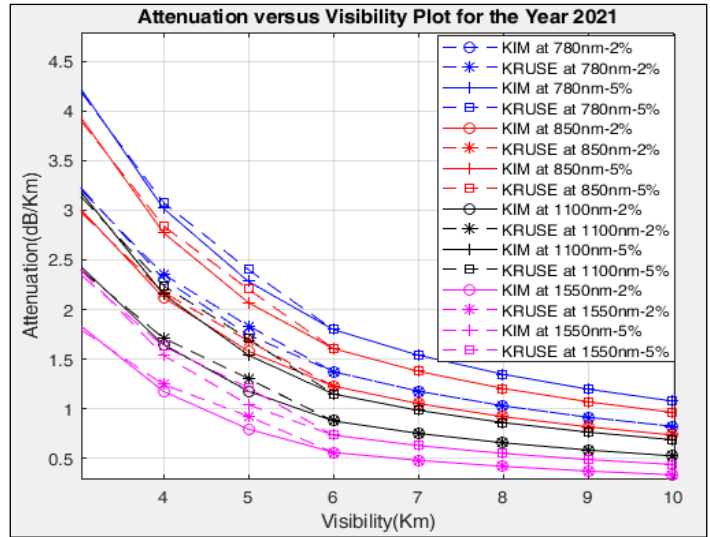


Figure 16: Combined attenuation plot when τ_{th} is at 2% and 5% for the year 2019. Source: Authors, (2023).

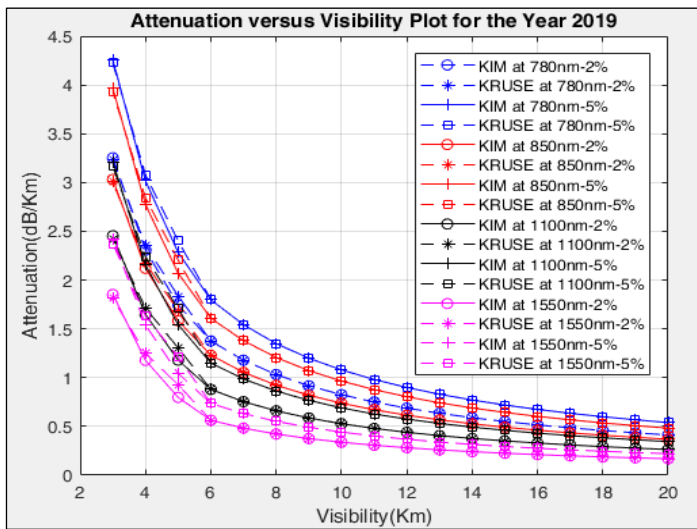


Figure 14: Combined attenuation plot when τ_{th} is at 2% and 5% for the year 2019. Source: Authors, (2023).

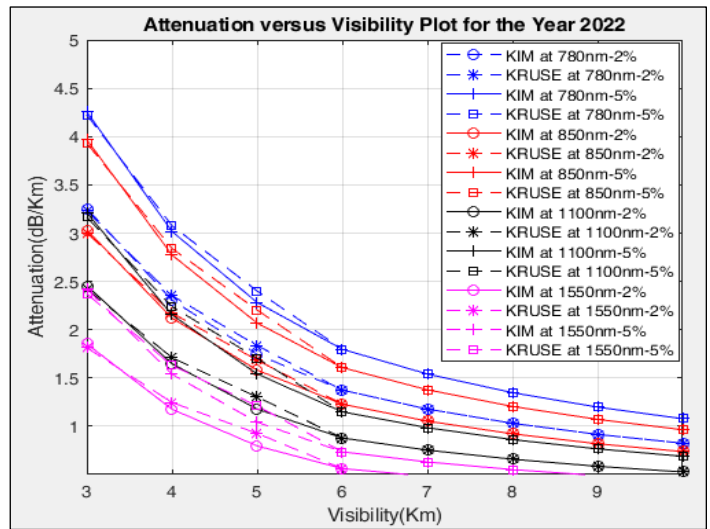


Figure 17: Combined attenuation plot when τ_{th} is at 2% and 5% for the year 2019. Source: Authors, (2023).

IV.2 NON-SELECTIVE SCATTERING

IV.2.1 Conversion Factor

The Rain data obtained has a precipitation interval of 1 hour. This scale does not adequately provide a proper window for investigation. In order to verify the authenticity of the data and form an adaptive time-series data, a conversion factor was developed. Terrestrial data taken on site at the Department of Physics, The Federal University of Technology, Akure was plotted against the available data. This is necessary because conversion factor is dependent on the location. Fig.5 shows the regression plot of conversion. To check for congruence in the data, the Root Mean Square (RMSE) value was calculated to be 0.022123154 and the chi-square value was obtained as 1.

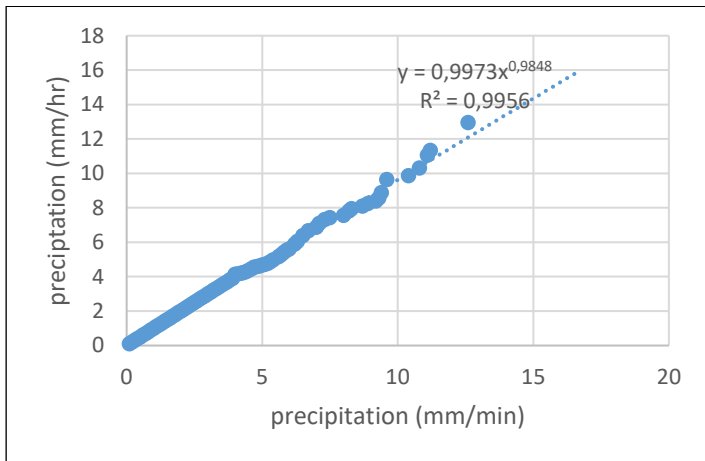


Figure 18: The regression plot of Rain Conversion.
Source: Authors, (2023).

IV.2.2 Examination of the Selected Rain Models

The rain intensity values were examined using the selected rain models. Fig. 6 provides the Rain attenuation (dB/km) against Rain intensity (mm/min) plot of the three models. It is clearly observed that the Suriza et al model shows close results to that of ITU-R model.

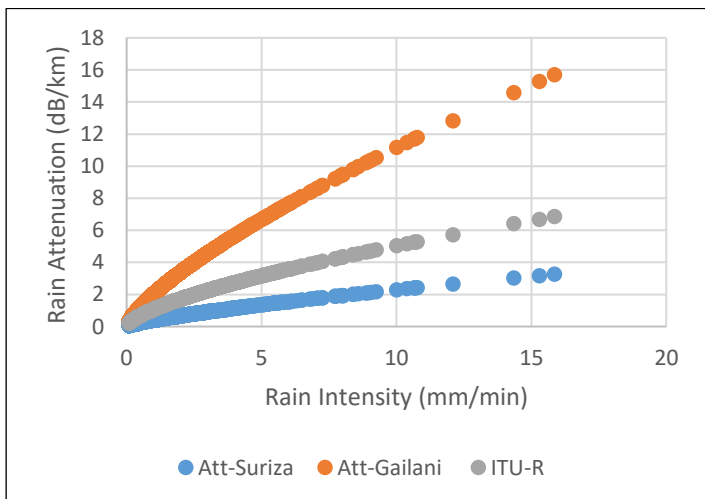


Figure 19: Rain Attenuation plots.
Source: Authors, (2023).

V. CONCLUSIONS

In this paper, we were able to analyse selected FSO model for Mie scattering and Geometric scattering on obtained

atmospheric data of Akure, in the southern region of Nigeria. An examination of the Kim and Kruse model was carried out on the data at 2% transmission threshold with a comparison at 5% transmission threshold for 780nm, 850nm, 1100nm and 1550nm transmission windows. It was observed that in all the years the highest attenuation occurred at 780nm transmission window. For the Geometric scattering, the Suriza et al, Gailani et al and ITU-R (Carbonneau) Models were examined with Rain intensity data. The Suriza et al model gave the lowest attenuation result. Since this work is limited to certain models, and in order to further study the effects of the atmosphere on FSO communication in the southern region of Nigeria, an empirical study is recommended.

VI. AUTHOR'S CONTRIBUTION

Conceptualization: Samson A. Oyetunji, Ibukunoluwa A. Olajide and Wasiu O. Popoola.

Methodology: Samson A. Oyetunji and Ibukunoluwa A. Olajide.

Investigation: Ibukunoluwa A. Olajide.

Discussion of results: Samson A. Oyetunji and Ibukunoluwa A. Olajide, Yekeen O. Olasoji, and Muhammad Ijaz.

Writing – Original Draft: Ibukunoluwa A. Olajide.

Writing – Review and Editing: Ibukunoluwa A. Olajide, and Muhammad Ijaz.

Resources: Ibukunoluwa A. Olajide.

Supervision: Samson A. Oyetunji, Yekeen O. Olasoji, and Wasiu O. Popoola.

Approval of the final text: Ibukunoluwa A. Olajide, Samson A. Oyetunji, Yekeen O. Olasoji, Wasiu O. Popoola and Muhammad Ijaz.

VII. ACKNOWLEDGMENTS

The authors would like to acknowledge the input received from Prof. J. S. Ojo of the Department of Physics, The Federal University of Technology, Akure, Nigeria.

VIII. REFERENCES

- [1] H. Henniger, and O. Wilfert, "An Introduction to Free-space Optical Communications," *RadioEngineering*, vol.19 no 2, 2010.
- [2] Z. Ghassemlooy, and W. O. Popoola, "Terrestrial free-space optical communications," *InTech*, pp. 355-392, 2010
- [3] A.G. Alkholidi, and K. S. Altowij, "Free space optical communications—Theory and practices" In *Contemporary Issues in Wireless Communications*. InTech., 2014
- [4] H. Kaushal, V.K. Jain, and S. Kar, "Free space optical communication," Springer India, 2017.
- [5] M.A. Khalighi, and M. Uysal, "Survey on free space optical communication: A communication theory perspective," *IEEE Communications Surveys & Tutorials*, vol. 16 no 4, pp. 2231-2258, 2014.
- [6] H. Willebrand, and B.S. Ghuman" *Free space optics: enabling optical connectivity in today's networks*". SAMS publishing, Indiana, 2002.
- [7] K. Anbarasi, C. Hemanth, and R.G. Sangeetha, "A review on channel models in free space optical communication systems," *Optics and Laser Technology*, vol. 97, pp.161-171, 2017.
- [8] A. Malik, and P. Singh, "Free space optics: current applications and future challenges," *International Journal of Optics*, Hindawi Publishing Corporation, 2015.
- [9] E. J. McCartney, "Optics of the atmosphere: scattering by molecules and particles," John Wiley and Sons, Inc., New York, 1976.

- [10] I. I. Kim, B. McArthur, and E. J. Korevaar, "Comparison of laser beam propagation at 785 nm and 1550 nm in fog and haze for optical wireless communications," In *Optical Wireless Communications III International Society for Optics and Photonics*, vol. 4214, pp. 26-38, 2001.
- [11] H. Kaushal, and G. Kaddoum, "Optical communication in space: Challenges and mitigation techniques," *IEEE communications surveys & tutorials*, vol.19 no.1, pp. 57-96, 2017.
- [12] S. S. Muhammad, B. Flecker, E. Leitgeb, and M. Gebhart. "Characterization of fog attenuation in terrestrial free space optical links," *Optical engineering*, vol. 46 no. 6, 2007.
- [13] M. Ijaz, Z. Ghassemlooy, H. Le-minh, S. Zvanovec, J. Perez, J. Pesek, and O. Fiser, "Experimental validation of fog models for FSO under laboratory controlled conditions". *IEEE Personal Indoor and Mobile Radio Communication*, pp. 19-23, 2013.
- [14] A. Z. Suriza, I. M. Rafiqul, A. K. Wajdi, and A. W. Naji, "Proposed parameters of specific rain attenuation prediction for free space optics link operating in tropical region". *Journal of Atmospheric and Solar-Terrestrial Physics*, vol 94, pp.93-99, 2013.
- [15] S. A. Al-Gailani, A.B. Mohammad, U.U. Sheikh, and R. Q. Shaddad, "Determination of rain attenuation parameters for free space optical link in tropical rain". *Optik*, 125(4), pp.1575-1578, 2014.
- [16] S. A, Zabidi, M. R., Islam, W, Al-Khateeb, and A. W. Naji. "Analysis of rain effects on terrestrial free space optics based on data measured in tropical climate". *IIUM Engineering Journal*, vol.12 no. 5, 2012.